


## RESEARCH ARTICLE

# Multi-Person Position Estimation Based on Correlation Between Received Signals Using MIMO FMCW Radar

KOJI ENDO<sup>1</sup>, (Graduate Student Member, IEEE), TOMOHIRO ISHIKAWA<sup>2</sup>,  
KOHEI YAMAMOTO<sup>2</sup>, (Member, IEEE), AND TOMOAKI OHTSUKI<sup>1</sup><sup>2</sup>, (Senior Member, IEEE)

<sup>1</sup>Graduate School of Science and Technology, Keio University, Yokohama, Kanagawa 223-8522, Japan

<sup>2</sup>Department of Information and Computer Science, Keio University, Yokohama, Kanagawa 223-8522, Japan

Corresponding author: Tomoaki Ohtsuki (ohtsuki@ics.keio.ac.jp)


This work was supported by the Grant Keio Leading-Edge Laboratory of Science and Technology, Japan, under Grant KEIO-KLL-000030.

**ABSTRACT** By using Multiple-Input Multiple-Output (MIMO) Frequency Modulated Continuous Wave (FMCW) radar, a range-angle map can be obtained that displays the signal strength in two dimensions with respect to distance and angular directions. In this process, a threshold algorithm such as Constant False Alarm Rate (CFAR) is used to detect positions where the signal strength exceeds a certain threshold value, enabling position estimation of targets. Furthermore, a method has been proposed to use the curve length of the trajectory of the I/Q signal to emphasize the signal of the person's position on the range angle map. However, the conventional CFAR may cause false alarms when noise and clutter signals are strong. In this paper, we propose a new method for human location estimation using the MIMO FMCW radar. Comparing the reflected signals from people and clutter, we see that I/Q signal variations associated with human motion have little correlation with clutter from stationary objects or noise, and I/Q signal variations associated with clutter often have high correlation with signals at other positions. We focus on the fact that there are many positions where the clutter component signal has a high correlation, compared to the signal caused by a person. Using the correlation map that expresses the correlation between the received I/Q signals on the range-angle plane, we evaluated the characteristics of noise and clutter components from walls on the correlation map by standard deviation. As a result, we can remove strong noise and clutter components caused from near walls, thus improving the accuracy of object location estimation.

**INDEX TERMS** MIMO FMCW radar, correlation, localization.

## I. INTRODUCTION

Human detection radar systems have been widely studied and have attracted attention with human identification and the detection of biological signals such as respiration and heartbeat. Accurate estimation of a person's location is also becoming important to improve the accuracy of these detections [1], [2], [3], [4], [5], [6], [7], [8].

The associate editor coordinating the review of this manuscript and approving it for publication was Valentina E. Balas .

Multiple-Input Multiple-Output (MIMO) radar is a radar that can estimate the Direction of Arrival (DOA) by analyzing the received signal using an array antenna. MIMO Frequency Modulated Continuous Wave (FMCW) radar is an FMCW radar equipped with an array antenna. In addition to DOA, MIMO FMCW radar can estimate the distance between the radar and the object. These position information can be used for object identification [9], [10], activity recognition [11], [12], [13], and vital sign detection [14], [15], [16], [17], [18].

To estimate the position of an object using MIMO FMCW radar, a range angle map, which represents the signal strength

versus distance and angle, is generally calculated. The range angle map may incorrectly detect positions where the target object does not exist due to noise such as clutter. In addition, when there are multiple radars within the radar coverage area, mutual interference can be a problem [19]. Therefore, the radar system uses a threshold algorithm such as CFAR (Constant False Alarm Rate) [20], [21], [22], [23], [24], to detect the target signal. However, depending on the threshold value, the accuracy of object location estimation tends to deteriorate. This is because noise and clutter components can cause false alarms at locations where the target object does not exist. Therefore, if these noises can be reduced, the probability of false detection can be reduced.

As a previous study for human detection, there were studies using the standard deviation of time-series I/Q signals at each range angle bin of range angle maps [25], [26], [27]. Furthermore, as a method to suppress large clutter, the Curve Length (CL) method to estimate the length of the trajectory of I/Q signals [28], [29] was developed. The length of the I/Q signal trajectory extends in proportion to the displacement of the human biological signal and body motion and becomes shorter for stationary objects. Therefore, using this length to generate a range angle map would improve the Signal-to-Clutter Ratio (SCR). However, in the presence of strong noise and/or clutter components, this can lead to false alarms at undesired locations.

In this paper, we propose a new human location estimation method using MIMO FMCW radar to reduce noise caused by clutter components on range angle maps and to improve the accuracy of object location estimation. Comparing the reflected signals from people and clutter, we see that I/Q signal variations associated with human motion have little correlation with other positions' signals, and I/Q signal variations associated with clutter often have high correlation with other positions' signals. To take advantage of these features, we introduce a correlation map that expresses the correlation between the received I/Q signals on a map. The clutter component caused by a wall has the characteristic of showing many cells with high correlation on the correlation map. From the experimentally acquired data, we show that the proposed method can remove strong noise and clutter components caused by the vicinity of the wall and improve the accuracy of object location estimation.

This paper is organized as follows. Section I describes the research background of this study. Section II describes the principle of MIMO FMCW radar. In Section III, we explain the related research on the multiple-person detection using MIMO FMCW radar and the CFAR-based position estimation method for radar systems. Section IV describes the proposed method and Section V shows the experimental results of the proposed method. Finally, Section VI presents the conclusion of this paper.

## II. PRINCIPLE OF MIMO FMCW RADAR

In this section, we firstly explain the principle of the FMCW radar, and then explain that of the MIMO FMCW radar. The

FMCW radar is a radar that calculates the distance to a target by transmitting signals with the microwave frequency linearly swept and detecting the difference between the transmitted signal and the reflected signal from the target. Now, let  $f_c$  and  $B$  be the minimum sweep frequency and the bandwidth of the chirp, respectively. Also, let  $T_c$  be the sweep duration. In the FMCW radar, microwaves are transmitted by the transmit antenna, and the transmitted microwaves are reflected by an object. The reflected signal  $r(t)$  is then received by the receive antenna.

$$r(t) = A\{\cos(2\pi f_c(t-t_d) + \pi \frac{B}{T_c}(t-t_d)^2 + \phi(t-t_d))\}, \quad (1)$$

where  $A$  is the signal power and  $\phi(t)$  is the phase noise. Also,  $t_d$  is given as  $t_d = \frac{2R(t)}{c}$ , where  $R(t)$  is the range between the FMCW radar and the object, and  $c$  is the speed of the electromagnetic wave. The received signal is modulated into two signals with the phase difference of  $\pi/2$ , i.e., in-phase and quadrature signals. These two signals can be expressed as a complex signal  $y(t)$ .

$$y(t) = Ae^{j(2\pi f_b t + \Phi(t) + \Delta\phi(t))}, \quad (2)$$

where  $f_b = 2BR(t)/(cT_c)$ ,  $\Phi(t) = 2\pi f_c t_d + \pi B t_d^2 / T_c$ , and  $\Delta\phi(t) = \phi(t) - \phi(t - 2R/c)$ .

The MIMO FMCW radar is an FMCW radar that has  $N_{Tx}$  transmit antennas and  $N_{Rx}$  receive antennas [9], [10], [11], [12], [13], [14], [15], [16], [17], [18], [28]. The radar transmits orthogonal chirp signals from  $N_{Tx}$  transmit antennas and receives each signal at  $N_{Rx}$  receive antennas. As a result,  $N_{Tx} \times N_{Rx}$  received signals are obtained. This is equivalent to constructing  $N_{Tx} \times N_{Rx}$  virtual array antennas. When the reflected signal with the incident angle of  $\theta$  is received at the  $k$  th antenna of  $K$  virtual array antennas, the received signal  $y_k(t)$  is expressed as

$$y_k(t, \theta) = Ae^{j(2\pi f_b t + \Phi(t) + \Delta\phi(t) + \frac{2\pi}{\lambda} d_k \sin \theta)}, \quad (3)$$

where  $\lambda$  is the carrier wave wavelength, and  $d_k$  is the relative distance between the  $k$  th receive antenna and the reference point. By calculating the beamforming weight  $w_k$ , the received signal for a specific beam direction can be obtained as

$$Y(t, \theta) = \sum_{k=1}^K y_k(t, \theta) w_k. \quad (4)$$

## III. RELATED WORK

### A. MULTIPLE PERSON DETECTION USING MIMO FMCW RADAR

This section describes a previous study on human location estimation using MIMO FMCW radar. In the past, studies of human location estimation used the standard deviation of time-series I/Q signals at each range angle bin [25], [26], [27]. However, this method has the problem that the normalized value of the standard deviation is limited in the codomain range to a value between 0 and 1. This means that larger phase variations cannot result in a larger value

of the standard deviation [28]. The SCR cannot be increased because the standard deviation saturates as the motion of the target increases. Therefore, in [28], the Curve Length (CL) method is proposed to discriminate a stationary clutter from a person, based on the fact that the curve length of the I/Q signal trajectory is proportional to the person's biometric signal and body motion. Since a person is accompanied by a fixed phase shift due to biometric signals and body motion, by estimating this change, it is possible to discriminate stationary clutter, which ideally has a constant phase, from a person. Using this property, the curve length (CL), which is the length of variation of the I/Q signal on the I/Q plane within the coherent processing interval (CPI), is calculated for each specified distance and angle as follows:

$$CL = \sqrt{\sum_{\tau=2}^{T_M} ((I[\tau] - I[\tau-1])^2 + (Q[\tau] - Q[\tau-1])^2)}, \quad (5)$$

where  $T_M$  is the CPI,  $I[\tau]$  and  $Q[\tau]$  are the in-phase and quadrature signals at the specified distance, angle, and sampling time  $\tau$ , respectively. If the displacement due to target motion is large, the curve length of the trajectory of the I/Q signals becomes large. Therefore, this method improves the detection sensitivity of the phase variation caused by motion and improves the detection accuracy of the target in the range angle map.

In [28], the I/Q trajectories at the locations of persons and a wall are shown. In [28], the I/Q trajectories at the locations of persons is detected has a longer curve length due to the influence of biological signals such as respiration, heartbeat, and body motion, which cause larger phase fluctuations. On the other hand, the I/Q trajectory at the location of a wall shows less phase variation and a shorter curve length.

## B. TARGET POSITION ESTIMATION BY CFAR ON RADAR SYSTEMS

This section describes the Constant False Alarm Rate (CFAR) [20], [21], [22], [23], [24], which is an effective threshold algorithm in radar systems. In a radar system, a signal is compared to a threshold value to detect an object of interest. It is considered difficult to determine an appropriate threshold value for detection. In radar systems, a threshold value that not only maximizes the detection rate but also keeps the false alarm rate below a predetermined level is considered good.

CFAR is a thresholding algorithm that extracts peak values from the acquired signal that are considered to be detectable, and with the use of appropriate threshold coefficients, the resulting false alarm rate can be kept constant. One widely used CFAR algorithm is CA-CFAR (Cell Average-Constant False Alarm Rate). CA-CFAR is a technique that detects peak values with high power based on an adaptive threshold value. When detecting a target from a 2D position estimation map, CA-CFAR first sets the cell under the test (CUT) as shown in Fig. 1. Next, CA-CFAR calculates the average of the signal power of the training cells around the CUT. An important point here is that cells around the peak value tend to show high

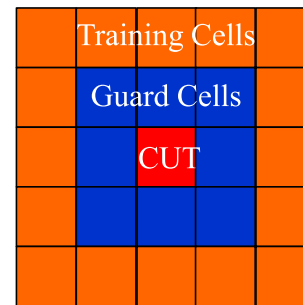


FIGURE 1. Diagram of CA-CFAR.

overall values because the power of the surrounding signals is also affected by the peak value. Therefore, guard cells are placed adjacent to the CUT. The threshold  $V_{th}$  for detection is calculated as follows:

$$V_{th} = \mu\alpha, \quad (6)$$

where  $\mu$  is the average signal power of the training cells and  $\alpha$  is a scaling factor. If the signal power of the CUT is greater than  $V_{th}$ , the cell is determined as “detected a target.” If the signal power of the CUT is less than  $V_{th}$ , the cell is determined as “did not detect a target.” After performing the above procedures for all the cells over a 2D position estimation map, we can obtain a detection map where “1” means the detected cell, and “0” means the cell that is not detected.

## C. PROBLEMS OF RELATED WORK

In this section, we describe the problems of the related studies described in the previous section, followed by an explanation of our proposed method.

In a related study, multiple persons were detected using a MIMO FMCW radar. By focusing on the curve length of the I/Q signals, wall clutters were suppressed and the person detection performance was improved. However, when noise and clutter components from walls remain strong, the power of the clutter signal exceeds that of the person position signal. Fig. 2 shows the result of the clutter suppression. Fig. 2 shows a range-angle map generated by the CL method, and the measurements were performed using the radar in Table 1, which is described later in Section V. For comparison, the range angle map without a person is shown in Fig 3. Figs. 2 and 3 show that clutter from the wall appears relatively strong even in the environments where the target is not present. In the presence of targets, a signal that appears to be a multipath component caused by a person is also generated. These noise, multipath, and clutter components need to be suppressed because they may cause false alarms when clutter is strong. In related work, [20] and [21] described a CFAR-based position estimation method for radar systems. This detection algorithm has been used and studied in recent studies [22], [23], [24]. However, depending on the threshold value, the accuracy of object detection may deteriorate. In particular, when noise and clutter components are strong, positions that they are not the targets may be

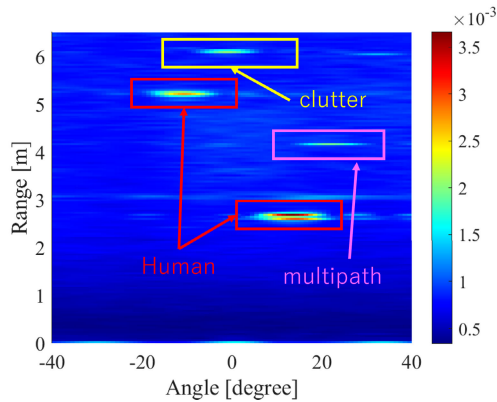


FIGURE 2. Range angle map using the CL method when the wall clutter is strong at 6.0 m and two people are at 2.5 m and 5.0 m.

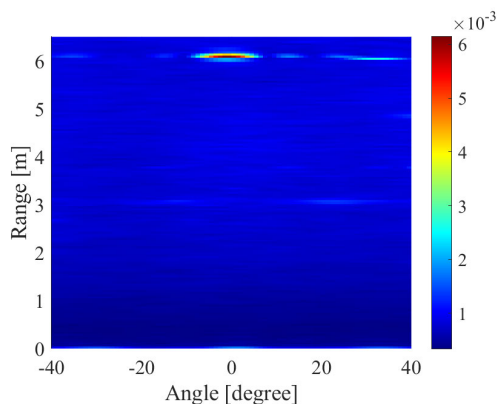


FIGURE 3. Range angle map using the CL method when the wall clutter is strong at 6.0 m without a person.

incorrectly detected. In other words, range angle maps with strong noise and clutter components may result in false alarms.

To solve this problem, a method to suppress the occurrence of false alarms by applying denoising using deep learning has been studied [30]. In [30], by applying Deep Image Prior (DIP) to the range angle maps, the noise generated in the case of short integration time is effectively reduced. This method reduces the occurrence of false alarms and improves the target detection performance. On the other hand, in strong clutter environments, the clutter could not be removed completely, resulting in little improvement in detection performance. Therefore, strong clutter must be reduced further to improve detection performance.

In this paper, we propose a new human location estimation method using MIMO FMCW radar to improve the accuracy of object location estimation. To achieve this objective, we focus on the large number of locations where the signal of the clutter component is highly correlated with the time variation of the signal caused by the clutter component. The algorithm incorporates a noise reduction method that takes advantage of the characteristics of noise and clutter. The algorithm is described below.

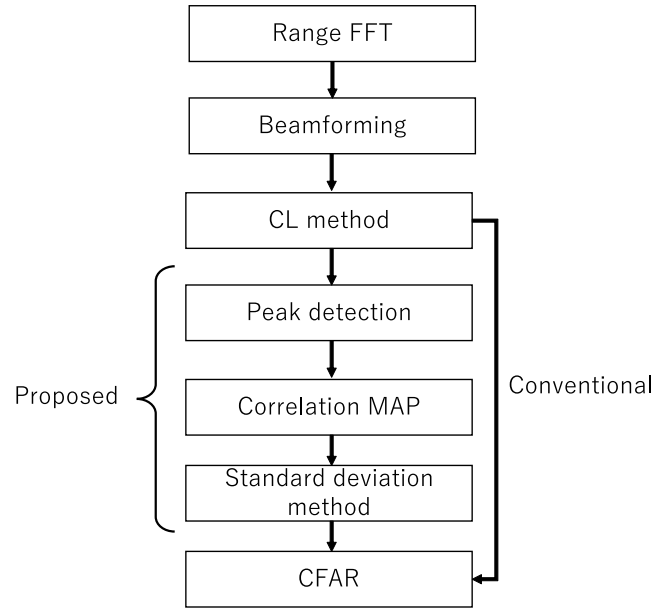


FIGURE 4. Flowchart of the proposed method.

#### IV. PROPOSED METHOD

The algorithm of the proposed method is shown in Fig. 4. The arrows on the outside in this figure show the flow of the conventional method. The algorithm of the proposed method is described in turn.

##### A. RANGE FFT (FAST FOURIER TRANSFORM)

Fast Fourier Transform (FFT) is performed along the measurement time for each antenna to obtain the distance between the radar and the target.

##### B. BEAMFORMING

The received signal for a particular beam direction is obtained by multiplying the beamforming weights. In this study, I/Q data is obtained for every 1° in the range from -40° to 40°.

##### C. GENERATE THE RANGE ANGLE MAP BY THE CL METHOD

Calculate the trajectory lengths of the I/Q signals on the I/Q plane at each range and angle and generate the range angle map. Fig. 5 shows a range angle map using the CL method.

##### D. PEAK DETECTION

Obtain the top  $n$  points of the cells with the highest power on the range angle map using the CL method.

##### E. GENERATE THE CORRELATION MAP

Fig. 6 shows the diagram of the correlation map calculation. We calculate the cross-correlation of time-varying I/Q signals between one of the previously acquired  $n$  points and all cells. By calculating the above, we can obtain the correlation map to check the correlation values on the range-angle plane. To highlight strongly correlated cells, only cells whose

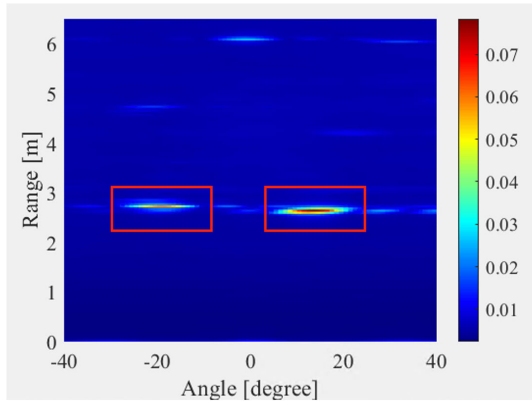


FIGURE 5. Range angle map using CL method with two subjects at 2.5 m.

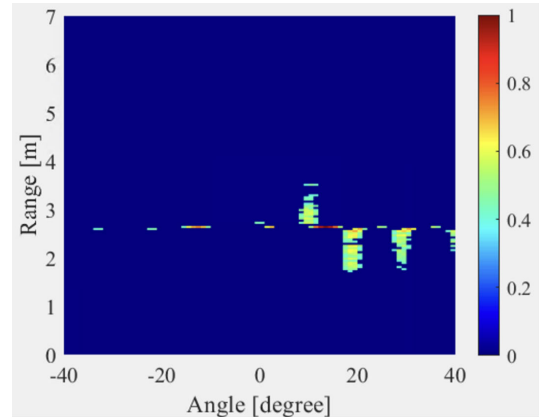


FIGURE 7. Correlation map between the position of the red square, which is the reference cell, and all the cells in Fig. 6.

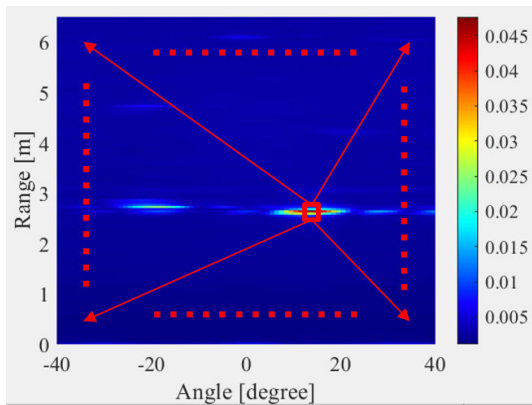


FIGURE 6. Diagram of correlation map calculation.

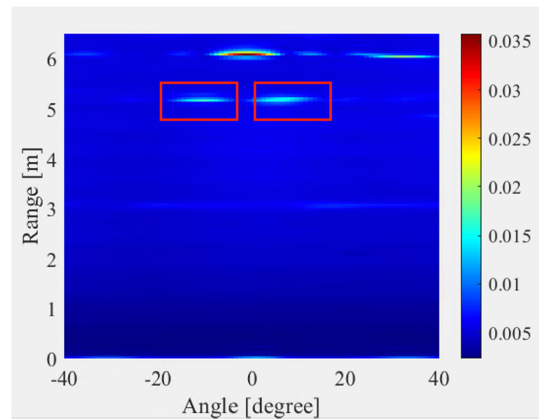


FIGURE 8. Range angle map using the CL method with two subjects at a distance of 5.0 m and angles of  $-10^\circ$  and  $10^\circ$ .

correlation values exceed a threshold  $C_{th}$  are extracted. In this way, only cells that are considered to be correlated with a reference point can be represented on the correlation map. This process is performed for all  $n$  points obtained, and a total of  $n$  correlation maps are output.

Fig. 7 shows a correlation map between the position of the red square, which is the reference cell in Fig. 6, and other areas. Here,  $C_{th}$  is set to 0.4 to differentiate the correlation maps of persons and clutter. As can be seen from this figure, the correlation map of human locations has many locations where the output value is 0 because I/Q signal variations associated with human motion have little correlation with clutter from stationary objects or noise. The locations where the output correlation value is greater than  $C_{th}$  are concentrated either at the location of the person or at different angles in the same distance as the location of the person. Since the locations correspond to range and angle sidelobes to the person's position, the I/Q signal at that location is considered to be strongly correlated with that at the person's position.

Next, we show the correlation map between the position of the clutter and other areas. Fig. 8 shows the range angle map when there are two subjects at a distance of 5.0 m and angles of  $-10^\circ$  and  $10^\circ$ . The wall is located at 6.0 m, and

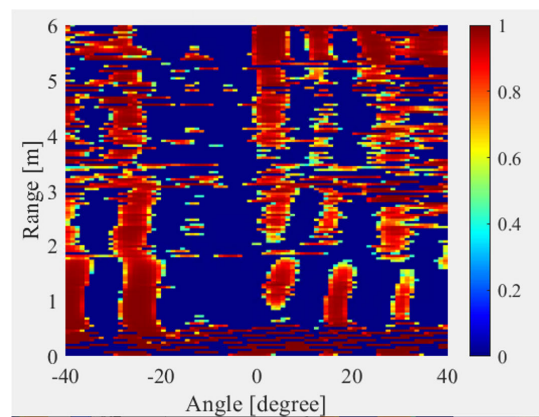


FIGURE 9. Correlation map of the clutter signal at a distance of 6.0 m and angle of  $0^\circ$  in Fig. 8.

the range angle map has two large clutters at  $0^\circ$  and  $40^\circ$  that would be mis-detected as human signals. A correlation map of the clutter signal at a distance of 6.0 m and an angle of  $0^\circ$  is shown in Fig. 9.

As can be seen from Fig. 9, the correlation map between the wall location and other areas has a high correlation value at many locations and shows large deviations in the correlation values, in contrast to the correlation map of the human-induced signal as shown in Fig. 7. Based on this difference, the next step is to improve the human detection performance on the range angle map.

#### F. STANDARD DEVIATION OF THE CORRELATION MAPS

To determine whether the reference cell is a person or a clutter from the correlation map, the standard deviation of the correlation map is calculated. We calculate the standard deviation using all correlation values on the correlation map. By calculating the standard deviation for all correlation maps,  $n$  standard deviations can be obtained. These  $n$  values correspond to the  $n$  points on the range angle map described in Section IV-D. As will be discussed later, the signals in the points where these standard deviations are low are more likely to be signals from human motion, and the signals in the points where they are high are more likely to be clutter signals. Let “std” be the standard deviation for one of the  $n$  points on the range angle map. For the cells that do not satisfy  $0 < \text{std} < SD_{th}$ , where  $SD_{th}$  is the threshold of the standard deviation, the power is set to 0 on the range angle map output by the CL method. By doing this, we can obtain a range angle map that reduces the influence of clutters. The reason is explained below.

For simplicity, we extend the  $n$  points selected in Section IV-D to all cells. The standard deviation of each correlation map is calculated, and the resulting standard deviation is projected onto the range angle plane to generate a standard deviation map. Two standard deviation maps are shown in Figs. 10 and 11. In Fig. 10, there are two persons at a distance of about 5.0 m and angles of  $-10^\circ$  and  $10^\circ$ . In Fig. 11, one person is at a distance of about 2.5 m and an angle of  $-20^\circ$ , and another is at a distance of about 5.0 m and an angle of about  $20^\circ$ . From these figures, it can be seen that the standard deviation maps show values below 0.1 at the positions where people are present and at the same distance as people. On the other hand, the standard deviation was 0.4 where the clutter is located. These indicate that the human or human-induced signal fits between  $0 < \text{std} < 0.1$ . Therefore,  $SD_{th}$  is set to 0.1. Since the cells that do not satisfy the above condition on the standard deviation map are not persons, the effect of clutter can be reduced by setting the values of cells at the same location on the range angle map to 0, as determined at the beginning of this section.

#### G. CFAR

If the value of the CUT exceeds the threshold  $V_{th}$ , the cell is determined to be detected. By determining for all the cells in the range angle map, the detection map such as Figs. 15 and 17 is obtained. In the detection map, locations where a person is present are indicated as 1 and locations where no person is present are indicated as 0.

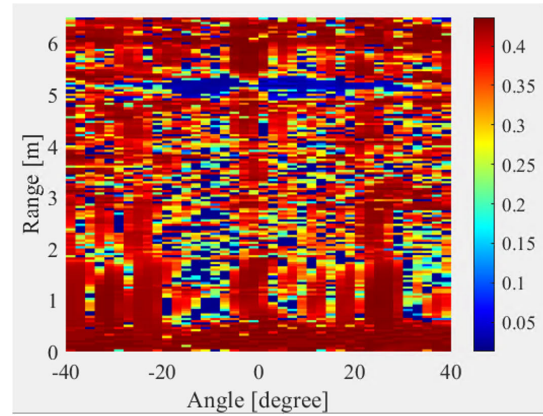


**FIGURE 10.** Standard deviation map for two subjects at a distance of approximately 5.0 m and at angles of  $-10^\circ$  and  $10^\circ$ . The colors indicate the standard deviation values.

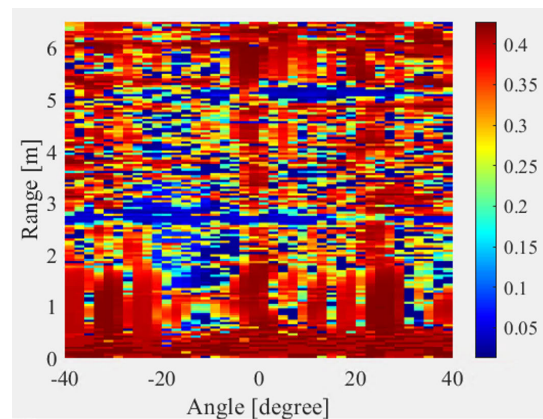


**FIGURE 11.** Standard deviation map with the subject at a distance of about 2.5 m and an angle of about  $-20^\circ$ , and at a distance of about 5.0 m and an angle of about  $20^\circ$ . The colors indicate the standard deviation values.

### V. EXPERIMENTAL EVALUATION

To evaluate the performance of the proposed method, we conducted experiments to estimate the location of persons in an indoor environment. Informed consent was obtained from all subjects prior to the experiments. In this section, we first describe the experimental specifications and then present the experimental results.

#### A. EXPERIMENTAL SPECIFICATIONS

A 79 GHz MIMO FMCW radar with 12 virtual element antennas was used in the experiments. Table 1 lists the radar specifications. The MIMO FMCW radar used in this experiment consists of a linear array of three transmitting antennas and four receiving antennas. The distance between two adjacent transmit antennas is twice the wavelength. The distance between adjacent receive antennas is half wavelength. When chirp signals are transmitted from each transmit antenna in turn and received by each receive antenna, 12 chirp signals are obtained. These signals are the same as those received by the 12 receiving linear array antennas. In the experiment, the radar was oriented horizontally so

TABLE 1. Radar specifications.

Item	Value
Start frequency	77.05 GHz
Modulation method	FMCW
Number of transmitting antennas	3
Number of receiving antennas	4
Bandwidth	3.4391 GHz
Range resolution	0.0436 m
Angular resolution	8.5 °
Velocity resolution	0.1449 m/s
Transmitting power	20 dBm (EIRP)
Sampling rate	160 Hz
CPI	12 s

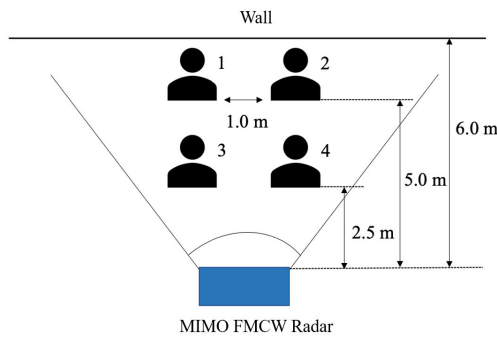


FIGURE 12. Experimental configuration.

TABLE 2. CA-CFAR parameters.

Item	Value
Guard cell length (distance)	3 cells, 0.13 m
Guard cell length (angle)	7 cells, 7°
Training cell length (distance)	5 cells, 0.22 m
Training cell length (angle)	7 cells, 7°

that the linear array antennas of the MIMO FMCW radar were positioned horizontally. Fig. 12 shows the experimental configuration. Figs. 13 and 14 show the experimental environment. In the experiment, two subjects sat in two different positions, “1”, “2”, “3”, and “4”, as shown in Fig. 12. MIMO FMCW Radar can detect multiple targets simultaneously because it can obtain signals for each range and angle by generating range angle maps. We chose the above location to simplify the evaluation of target detection performance in subsequent evaluations. The positions 1 and 2 were about 5.0 m from the radar, and the positions 3 and 4 were about 2.5 m from the radar. Informed consent was obtained from all subjects before experimenting. The distance between the positions 1 and 2, 3 and 4 was about 1.0 m. There was a wall at about 6.0 m from the radar. Table 2 shows the CA-CFAR parameters. The performance of the proposed method was evaluated based on these parameters.

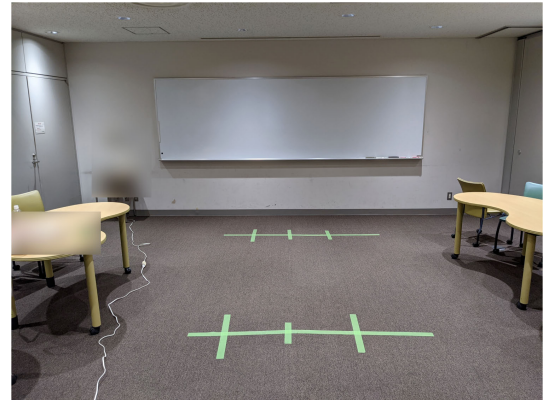


FIGURE 13. Experimental environment (Subjects side).



FIGURE 14. Experimental environment (Radar side).

**B. DEFINITIONS FOR EVALUATION**

To evaluate the performance of the proposed method, we first define “detection” and “false alarm.” Fig. 15 is the detection map after applying CFAR. First, the areas where the targets were present in each experimental configuration are set as shown in the red box. If there is a point detected as a target in the red box, the detection map is defined as “detection.” If there is a point detected as a target outside the red box, the detection map is defined as “false alarm.” The size of the red box is set to an angle of about 20 degrees and a distance of about 20 cm.

Next, based on the above definitions, we define the detection rate  $P_d$  and false alarm rate  $P_{fa}$  as follows:

$$P_d = \frac{N_d}{N_m}, \tag{7}$$

$$P_{fa} = \frac{N_{fa}}{N_m}, \tag{8}$$

where  $N_d$  is the number of range angle maps determined as “detection,”  $N_{fa}$  is the number of range angle maps determined as “false alarm,” and  $N_m$  is the total number of range angle maps. Because there were two people as targets, one range angle map was calculated as 1 if both targets were detected, 0.5 if only one target was detected,

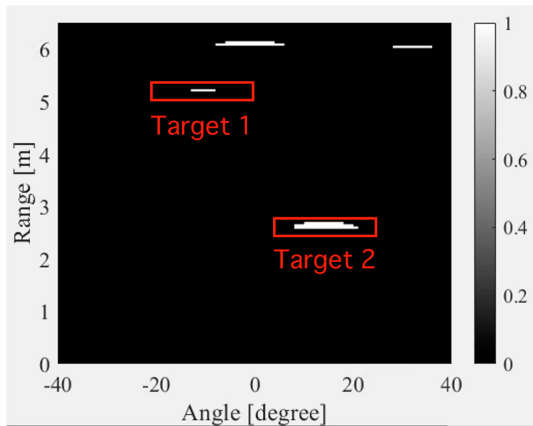


FIGURE 15. How to determine “detection” and “false alarm.”

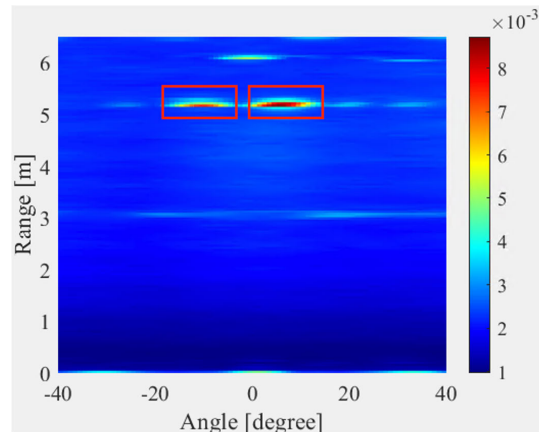


FIGURE 16. Range angle map using the CL method.

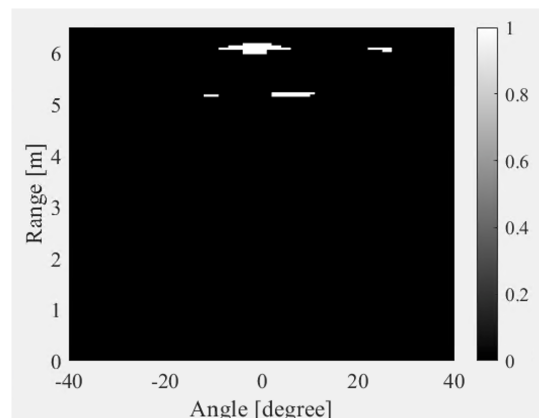
and 0 if neither was detected. In calculating  $N_d$ , the sum of above values was taken as  $N_d$ . One range angle map was generated using 12 seconds of data. Since the measurement time was 60 seconds for each location, 13 range angle maps were generated in 4 second steps for each measurement. We calculated the detection rate  $P_d$  and the false alarm rate  $P_{fa}$  using  $N_m = 13$  range angle maps when the CFAR scaling factor  $\alpha$  was varied from 1.0 to 9.9 by 0.1 steps. The resulting 90 combinations of  $P_d$  and  $P_{fa}$  were used to obtain Receiver Operating Characteristic (ROC) curves. Furthermore, the Area Under Curve (AUC), which represents the area under the ROC curve, was calculated and compared between the proposed method, the conventional method shown in Fig. 4, and the denoising method with DIP described in Section III-C. Here, the conventional method refers to a method to detect targets by generating the range angle maps using the CL method [28] and applying CA-CFAR as is.

C. EXPERIMENTAL RESULTS

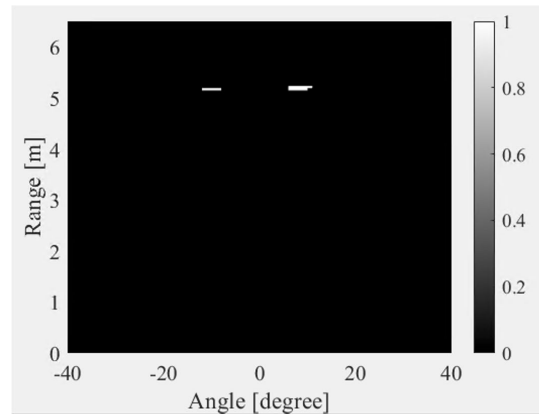
Fig. 16 shows the range angle map using the CL method for the case where the subjects were at positions 1 and 2 in Fig. 13. In Fig. 16, there are two positions with strong cell power at 5.0 m, corresponding to two subjects. We can also see a large clutter at the 6.0 m, corresponding to the wall location. This clutter may unintentionally cause a detection in the detection map after applying CA-CFAR.

Fig. 17 shows (a) The detection map generated by the conventional method and (b) by the proposed method. To generate Fig. 17,  $\alpha$  was set to 1.9. As mentioned above, “1” is a detected cell and “0” is a cell that is not detected in the detection map. In Fig. 17(a), there are two detected regions near 6.0 m where no one exists. On the other hand, no such false alarms are observed in Fig. 17(b). These results indicate that the proposed method can reduce the effects of clutter components that may cause false alarms.

Next, the detection rate  $P_d$  and the false alarm rate  $P_{fa}$  were calculated using 13 range angle maps for each of the conventional, proposed, and denoising methods when  $\alpha$  was varied from 1.0 to 9.9. Then, 90 combinations of  $P_d$



(a) The detection map generated by the conventional method.



(b) The detection map generated by the proposed method.

FIGURE 17. Comparison of the detection maps ( $\alpha = 1.9$ ) generated by (a) the conventional method, (b) the proposed method, where “1” means the detected cell, and “0” means the cell that is not detected.

and  $P_{fa}$  were plotted on the  $P_d - P_{fa}$  plane to draw the ROC curves. The AUC of the ROC curves was calculated for the conventional method, the proposed method, and the denoising method, and is shown in Table 3.  $n$  in the proposed method represents the number of cells with the highest power selected to generate the correlation map described in Section IV-D and IV-E. As shown in Table 3, the proposed



**TABLE 3. AUC of the conventional method and the proposed method using 12 seconds of measurement data ( $n$ : the number of the extraction points).**

Target positions	Conventional	Proposed( $n = 70$ )	( $n = 80$ )	( $n = 90$ )	( $n = 100$ )	Denoising (DIP)
(1,2)	0.77	0.93	0.94	0.94	0.95	0.92
(1,3)	0.82	0.91	0.92	0.92	0.92	0.92
(1,4)	0.92	0.95	0.95	0.95	0.94	0.92
(2,3)	0.72	0.80	0.80	0.81	0.81	0.81
(2,4)	0.92	0.99	0.99	0.99	0.99	0.92
(3,4)	0.97	1.00	1.00	1.00	1.00	0.99
Ave.	0.85	0.93	0.93	0.94	0.94	0.92

**TABLE 4. AUC of the conventional method and the proposed method using 5 second integration ( $n$ : the number of the extraction points).**

Target positions	Conventional	Proposed( $n = 70$ )	( $n = 80$ )	( $n = 90$ )	( $n = 100$ )
(1,2)	0.59	0.88	0.89	0.89	0.90
(1,3)	0.79	0.87	0.90	0.91	0.91
(1,4)	0.89	0.86	0.87	0.88	0.88
(2,3)	0.69	0.74	0.74	0.74	0.73
(2,4)	0.85	0.87	0.88	0.90	0.90
(3,4)	0.92	0.96	0.96	0.96	0.96
Ave.	0.79	0.86	0.87	0.88	0.88

**TABLE 5. AUC for the conventional method and the proposed method using 20 second integration ( $n$ : the number of the extraction points).**

Target positions	Conventional	Proposed( $n = 70$ )	( $n = 80$ )	( $n = 90$ )	( $n = 100$ )
(1,2)	0.80	0.92	0.93	0.95	0.97
(1,3)	0.83	0.98	0.98	0.98	0.99
(1,4)	0.90	0.94	0.94	0.94	0.94
(2,3)	0.78	0.85	0.87	0.88	0.88
(2,4)	0.89	0.92	0.92	0.92	0.92
(3,4)	0.97	1.00	1.00	1.00	1.00
Ave.	0.86	0.94	0.94	0.95	0.95

method improves the conventional method in all positions, regardless of the value of  $n$ . A notable case is when the subject positions were (1, 2). This configuration was when clutter strongly occurred at the 6.0 m position, as shown in Fig. 16. The proposed method reduced the effect of clutter and improved the AUC by about 23% at maximum. In addition, the AUC improves in many cases as  $n$ , the number of the extraction points of cells with high power, increases on the range angle map using the CL method. This result shows a trade-off between the calculation time and the detection performance since the calculation time increases as the number of the extraction points increases. It can be confirmed that the AUC of the proposed method when  $n$  is 100 is higher than that of the denoising method with DIP, the latest target detection method.

Next, we check the AUC when the integration time to generate the range angle map is shorter or longer than 12 seconds. We set up the following cases for shorter and longer integration times.

- 5 second integration with 5 second steps, 12 range angle maps.

- 20 second integration with 5 second steps, 9 range angle maps.

The detection rate  $P_d$  and the false alarm rate  $P_{fa}$  were calculated using the above number of range angle maps. The ROC curve was then drawn in the same manner and the AUC was calculated. Table 4 shows the AUC of the conventional method and the proposed method using 5 second integration, and Table 5 shows the AUC of the conventional method and the proposed method using 20 second integration. As can be seen from these tables, the average AUC of the proposed method for both 5 and 12 seconds of integration time is improved over the conventional method. As in the case of the 12 seconds integration, the clutter was strong at the subject positions (1, 2), so the proposed method improves the AUC significantly.

Next, the relationship between the number of the extraction points and AUC is shown. From the results of Table 3, Table 4, and Table 5, we know that the AUC value improves as the number of the extraction points increases. This result was confirmed by increasing the number of the extraction points not only to 100 but also to 200. Fig. 18 shows the relationship

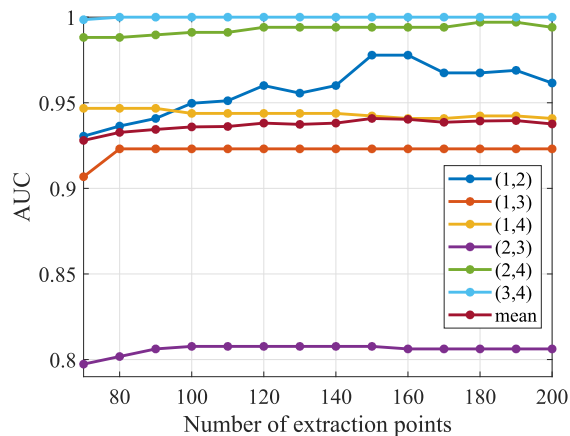


**FIGURE 18.** Relationship between the number of the extraction points and the AUC in 12 seconds of measurement time.

between the number of the extraction points and the AUC of the cells with high power on the range angle map using the CL method at a measurement time of 12 seconds. From this figure, the AUC is flat or slightly increasing except at the subject positions (1, 2), which are indicated by the blue line. On the other hand, at the subject's position (1, 2), the AUC tends to improve with increasing  $n$ . This condition is where clutter was strong, as described above. Considering the real environment, it is possible that clutter may be strong and that the number of clutter may increase. Considering these points, it is expected that the detection accuracy will be greatly improved by increasing the number of the extraction points in the real environment, rather than in the environment where the location of walls and other objects is known, as was used in this study.

## VI. CONCLUSION

This paper proposes a new method for estimating human positions using MIMO FMCW radar to reduce noise due to clutter components on range angle maps. Focusing on the correlation of I/Q signals at each distance and angle, we proposed a method to distinguish between signals caused by humans and those caused by clutter. The proposed method takes advantage of the fact that signals caused by clutter components have a large number of highly correlated cells on the correlation map, while signals caused by humans have only a small number of highly correlated cells at the same distance. The correlation map, which expresses the correlation between received I/Q signals on the range-angle plane, was introduced, and the clutter on the range angle map was reduced by evaluating the characteristics of clutter components from walls on the correlation map by their standard deviations. As a result, the proposed method improved the AUC by more than about 23% compared to the conventional method in the case of strong clutter near the wall, and the proposed method improved the average AUC by more than about 3% compared to the conventional method in the case of no strong clutter.

## REFERENCES

- [1] J. Yan, G. Zhang, H. Hong, H. Chu, C. Li, and X. Zhu, "Phase-based human target 2-D identification with a mobile FMCW radar platform," *IEEE Trans. Microw. Theory Techn.*, vol. 67, no. 12, pp. 5348–5359, Dec. 2019.
- [2] L. Ren, Y. S. Koo, H. Wang, Y. Wang, Q. Liu, and A. E. Fathy, "Noncontact multiple heartbeats detection and subject localization using UWB impulse Doppler radar," *IEEE Microw. Wireless Compon. Lett.*, vol. 25, no. 10, pp. 690–692, Oct. 2015.
- [3] S. G. Kim, I. C. Ko, and S. H. Jung, "High resolution CMOS IR-UWB radar for non-contact human vital signs detection," in *Proc. IEEE Radio Freq. Integr. Circuits Symp. (RFIC)*, Aug. 2020, pp. 27–30, doi: 10.1109/RFIC49505.2020.9218284.
- [4] K. Gupta, M. B. Srinivas, J. Soumya, O. J. Pandey, and L. R. Cenkaramaddi, "Automatic contact-less monitoring of breathing rate and heart rate utilizing the fusion of mmWave radar and camera steering system," *IEEE Sensors J.*, vol. 22, no. 22, pp. 22179–22191, Nov. 2022, doi: 10.1109/JSEN.2022.3210256.
- [5] D. Kocur, T. Porteleky, and M. Svecová, "UWB radar testbed system for localization of multiple static persons," in *Proc. IEEE SENSORS*, Oct. 2019, pp. 1–4, doi: 10.1109/SENSORS43011.2019.8956782.
- [6] H. Lee, B.-H. Kim, and J.-G. Yook, "Path loss compensation method for multiple target vital sign detection with 24-GHz FMCW radar," in *Proc. IEEE Asia-Pacific Conf. Antennas Propag. (APCAP)*, Aug. 2018, pp. 100–101, doi: 10.1109/APCAP.2018.8538182.
- [7] J. Liu, Y. Li, C. Li, C. Gu, and J.-F. Mao, "Accurate measurement of human vital signs with linear FMCW radars under proximity stationary clutters," *IEEE Trans. Biomed. Circuits Syst.*, vol. 15, no. 6, pp. 1393–1404, Dec. 2021, doi: 10.1109/TBCAS.2021.3123830.
- [8] G. Li, Y. Ge, Y. Wang, Q. Chen, and G. Wang, "Detection of human breathing in non-line-of-sight region by using mmWave FMCW radar," *IEEE Trans. Instrum. Meas.*, vol. 71, pp. 1–11, 2022, doi: 10.1109/TIM.2022.3208266.
- [9] N. Knudde, B. Vandersmissen, K. Parashar, I. Couckuyt, A. Jalalvand, A. Bourdoux, W. De Neve, and T. Dhaene, "Indoor tracking of multiple persons with a 77 GHz MIMO FMCW radar," in *Proc. Eur. Radar Conf. (EURAD)*, Oct. 2017, pp. 61–64.
- [10] B. Vandersmissen, N. Knudde, A. Jalalvand, I. Couckuyt, and A. Bourdoux, "Indoor person identification using a low-power FMCW radar," *IEEE Trans. Geosci. Remote Sens.*, vol. 56, no. 7, pp. 3941–3952, Jul. 2018, doi: 10.1109/TGRS.2018.2816812.
- [11] Y. Kim, I. Alnujaim, and D. Oh, "Human activity classification based on point clouds measured by millimeter wave MIMO radar with deep recurrent neural networks," *IEEE Sensors J.*, vol. 21, no. 12, pp. 13522–13529, Jun. 2021, doi: 10.1109/JSEN.2021.3068388.
- [12] F. Aziz, O. Metwally, P. Weller, U. Schneider, and M. F. Huber, "A MIMO radar-based metric learning approach for activity recognition," in *Proc. IEEE Radar Conf. (RadarConf)*, Mar. 2022, pp. 1–6, doi: 10.1109/RADARCONF2248738.2022.9764202.
- [13] W. Lei, X. Jiang, Q. Tan, L. Xu, Y. Zhao, T. Xu, Y. Li, Q. Gu, G. Liu, Y. Zhao, and W. Li, "A TD-CF preprocessing method of FMCW radar for dynamic hand gesture recognition," in *Proc. IEEE Int. Conf. Signal, Inf. Data Process. (ICSIDP)*, Dec. 2019, pp. 1–5, doi: 10.1109/ICSIDP47821.2019.9173196.
- [14] K. Yamamoto, K. Endo, and T. Ohtsuki, "Remote sensing of heartbeat based on space diversity using MIMO FMCW radar," in *Proc. IEEE Global Commun. Conf. (GLOBECOM)*, Dec. 2021, pp. 1–6, doi: 10.1109/GLOBECOM46510.2021.9685033.
- [15] T. Koda, T. Sakamoto, S. Okumura, and H. Taki, "Noncontact respiratory measurement for multiple people at arbitrary locations using array radar and respiratory-space clustering," *IEEE Access*, vol. 9, pp. 106895–106906, 2021, doi: 10.1109/ACCESS.2021.3099821.
- [16] M. Alizadeh, G. Shaker, and S. Safavi-Naeini, "Remote health monitoring system for bedbound patients," in *Proc. IEEE 20th Int. Conf. Bioinf. Bioeng. (BIBE)*, Oct. 2020, pp. 801–806, doi: 10.1109/BIBE50027.2020.001136.
- [17] W. Wang, Y. Wang, M. Zhou, and W. Nie, "A novel vital sign sensing algorithm for multiple people detection based on FMCW radar," in *Proc. IEEE Asia-Pacific Microw. Conf. (APMC)*, Dec. 2020, pp. 1104–1106, doi: 10.1109/APMC47863.2020.9331552.
- [18] B. R. Upadhyay, A. B. Baral, and M. Torlak, "Vital sign detection via angular and range measurements with mmWave MIMO radars: Algorithms and trials," *IEEE Access*, vol. 10, pp. 106017–106032, 2022, doi: 10.1109/ACCESS.2022.3211527.

- [19] Z. Xu, "Bi-level  $\ell_1$  optimization-based interference reduction for millimeter wave radars," *IEEE Trans. Intell. Transp. Syst.*, early access, Oct. 25, 2022, doi: [10.1109/TITS.2022.3215636](https://doi.org/10.1109/TITS.2022.3215636).
- [20] H. Rohling, *Introduction to RADAR Systems*, 3rd ed. New York, NY, USA: McGraw-Hill, 2008.
- [21] H. Rohling, "Radar CFAR thresholding in clutter and multiple target situations," *IEEE Trans. Aerosp. Electron. Syst.*, vols. AES-19, no. 4, pp. 608–621, Jul. 1983.
- [22] D. Lühr and M. Adams, "Radar noise reduction based on binary integration," *IEEE Sensors J.*, vol. 15, no. 2, pp. 766–777, Feb. 2015, doi: [10.1109/JSEN.2014.2352295](https://doi.org/10.1109/JSEN.2014.2352295).
- [23] W. Dong, T. Sun, J. Tian, J. Wang, Z. Song, and Q. Fu, "A target location algorithm based on millimeter wave radar," in *Proc. IEEE 6th Inf. Technol. Mechatronics Eng. Conf. (ITOEC)*, Mar. 2022, pp. 646–651, doi: [10.1109/ITOEC53115.2022.9734670](https://doi.org/10.1109/ITOEC53115.2022.9734670).
- [24] L. P. Jimenez Jimenez, F. D. A. Garcia, M. C. L. Alvarado, G. Fraidenaich, and E. R. D. Lima, "A general CA-CFAR performance analysis for weibull-distributed clutter environments," *IEEE Geosci. Remote Sens. Lett.*, vol. 19, 2022, Art. no. 4025305, doi: [10.1109/LGRS.2022.3187554](https://doi.org/10.1109/LGRS.2022.3187554).
- [25] G. Wang, C. Gu, T. Inoue, and C. Li, "A hybrid FMCW-interferometry radar for indoor precise positioning and versatile life activity monitoring," *IEEE Trans. Microw. Theory Techn.*, vol. 62, no. 11, pp. 2812–2822, Nov. 2014.
- [26] Z. Peng, J. M. Munoz-Ferreras, Y. Tang, C. Liu, R. Gomez-Garcia, L. Ran, and C. Li, "A portable FMCW interferometry radar with programmable low-IF architecture for localization, ISAR imaging, and vital sign tracking," *IEEE Trans. Microw. Theory Techn.*, vol. 65, no. 4, pp. 1334–1344, Apr. 2017.
- [27] Z. Peng, L. Ran, and C. Li, "A K-band portable FMCW radar with beamforming array for short-range localization and vital-Doppler targets discrimination," *IEEE Trans. Microw. Theory Techn.*, vol. 65, no. 9, pp. 3443–3452, Sep. 2017, doi: [10.1109/TMTT.2017.2662680](https://doi.org/10.1109/TMTT.2017.2662680).
- [28] K. Han and S. Hong, "Detection and localization of multiple humans based on curve length of I/Q signal trajectory using MIMO FMCW radar," *IEEE Microw. Wireless Compon. Lett.*, vol. 31, no. 4, pp. 413–416, Apr. 2021.
- [29] K. Han and S. Hong, "MIMO monopulse radar for detecting human targets with I/Q curve-length estimations," *IEEE Microw. Wireless Compon. Lett.*, vol. 32, no. 3, pp. 214–217, Mar. 2022, doi: [10.1109/LMWC.2022.3142322](https://doi.org/10.1109/LMWC.2022.3142322).
- [30] K. Endo, K. Yamamoto, and T. Ohtsuki, "A denoising method using deep image prior to human-target detection using MIMO FMCW radar," *Sensors*, vol. 22, no. 23, p. 9401, Dec. 2022, doi: [10.3390/S22239401](https://doi.org/10.3390/S22239401).



**KOHEI YAMAMOTO** (Member, IEEE) received the B.E., M.E., and Ph.D. degrees from Keio University, Yokohama, Japan, in 2017, 2019, and 2021, respectively. He is currently working as an Assistant Professor with Keio University. His research interests include signal processing, machine learning, and their applications, especially in biomedical engineering. He is a member of IEICE.



**TOMOAKI OHTSUKI** (Senior Member, IEEE) received the B.E., M.E., and Ph.D. degrees in electrical engineering from Keio University, Yokohama, Japan, in 1990, 1992, and 1994, respectively. From 1993 to 1995, he was a Special Researcher of Fellowships of the Japan Society for the Promotion of Science for Japanese Junior Scientists. From 1994 to 1995, he was a Postdoctoral Fellow and a Visiting Researcher of electrical engineering at Keio University.

From 1995 to 2005, he was with the Science University of Tokyo. From 1998 to 1999, he was with the Department of Electrical Engineering and Computer Sciences, University of California at Berkeley, Berkeley, CA, USA. In 2005, he joined Keio University, where he is currently a Professor. He has published more than 235 journal articles and 470 international conference papers. He gave tutorials and keynote speeches at many international conferences, including IEEE VTC, IEEE PIMRC, and IEEE WCNC. His research interests include wireless communications, optical communications, signal processing, and information theory. He is a fellow of IEICE and a member of the Engineering Academy of Japan. He was a recipient of the 1997 Inoue Research Award for Young Scientist, the 1997 Hiroshi Ando Memorial Young Engineering Award, the 2000 Ericsson Young Scientist Award, the 2002 Funai Information and Science Award for Young Scientist, IEEE the 1st Asia-Pacific Young Researcher Award in 2001, the 5th International Communication Foundation (ICF) Research Award, the 2011 IEEE SPCE Outstanding Service Award, the 27th TELECOM System Technology Award, *ETRI Journal* 2012 Best Reviewer Award, the 9th International Conference on Communications and Networking in China in 2014 (CHINACOM 2014) Best Paper Award, the 2020 Yagami Award, and the 26th Asia-Pacific Conference on Communications (APCC 2021) Best Paper Award. He served as the Chair for the IEEE Communications Society, Signal Processing for Communications and Electronics Technical Committee. He has served as the General Co-Chair, the Symposium Co-Chair, and the TPC Co-Chair for many conferences, including IEEE GLOBECOM 2008, SPC, IEEE ICC 2011, CTS, IEEE GLOBECOM 2012, SPC, IEEE ICC 2020, SPC, IEEE APWCS, IEEE SPAWC, and IEEE VTC. He was the Vice President and the President of the Communications Society of the IEICE. He is also serving as the Asia-Pacific Board Director for IEEE Communications Society. He served as a Technical Editor for the *IEEE Wireless Communications Magazine* and an Editor for *Physical Communications* (Elsevier). He is also serving as an Area Editor for the IEEE TRANSACTIONS ON VEHICULAR TECHNOLOGY and an Editor for the IEEE COMMUNICATIONS SURVEYS AND TUTORIALS. He is a Distinguished Lecturer of IEEE.



**KOJI ENDO** (Graduate Student Member, IEEE) received the B.E. degree from the Nagoya Institute of Technology, Nagoya, Japan, in 2006, and the M.E. degree from Nagoya University, Nagoya, in 2008. He is currently pursuing the Ph.D. degree with the Graduate School, Keio University. In 2008, he joined the Technical Research and Development Institute, Ministry of Defense, Japan, where he was engaged in the research of RF sensor systems. His research interest includes

array signal processing. He is a member of IEICE.

**TOMOHIRO ISHIKAWA** received the B.E. degree from the Faculty of Science and Technology, Keio University, in 2022.

• • •